Journal of Alloys and Compounds 509 (2011) 5295–5299

Contents lists available at ScienceDirect

Journal of Alloys and Compounds

journal homepage: www.elsevier.com/locate/jallcom

Red-emitting $Ln_{2-x}Eu_xTe_2O_6$:RE (Ln = La, Y; RE = Sm^{3+}, Gd^{3+}) phosphors prepared by the Pechini sol–gel method

Jaime Llanos[a,b,*], Rodrigo Castillo[a], Darío Espinoza[a], Rina Olivares[a], Ivan Brito[b]

[a] Departamento de Química, Universidad Católica del Norte, Avda. Angamos 0610, Casilla 1280, Antofagasta, Chile
[b] Departamento de Química, Universidad de Antofagasta, Campus Coloso, Antofagasta, Chile

ARTICLE INFO

Article history:
Received 28 July 2010
Received in revised form 20 January 2011
Accepted 20 January 2011
Available online 3 February 2011

Keywords:
Inorganic materials
Optical materials
Sol–gel processes
Optical properties
Photoluminescence

ABSTRACT

$La_{1.90}Eu_{0.10}TeO_6$:RE^{3+} (RE = Gd, Sm) and Y_2TeO_6:Eu^{3+} nanophosphors were prepared by the Pechini sol–gel process, using lanthanide sesquioxides and telluric acid as precursors. X-ray diffraction (XRD), scanning electron microscopy (SEM), photoluminescence spectra (PL) and fluorescence lifetime were used to characterize the resulting phosphors. The results of XRD indicate that all samples crystallized completely at 1073 K and are isostructural with orthorhombic Ln_2TeO_6. The SEM study reveals that the samples have a strong tendency to form agglomerates with an average size ranging from 40 to 65 nm. The luminescence decay curves suggest for all samples a monoexponential behavior. The photoluminescence intensity and chromaticity were improved for excitation at 395 nm when the co-doping concentration reaches the 1% mol. The optimized phosphors $La_{1.88}Eu_{0.10}Gd_{0.02}TeO_6$ and $La_{1.88}Eu_{0.10}Sm_{0.02}TeO_6$, could be considered an efficient red-emitting phosphor for solid-state lighting devices based on InGaN LEDs.

1. Introduction

Phosphors are also called luminescent materials. Luminescence is termed according to the nature of the excitation energy involved in the process. Various types of excitation sources may be used and in the last years, research in luminescent materials is well organized according to the excitation source. Luminescent materials in plasma display panels (PDP) and field emission displays (FED) use the high-energy side of the ultraviolet spectrum and even low voltage electrons, respectively. Phosphors in LED (light emitting diodes) and in fluorescent lamps are excited by near-UV or blue light [1]. The latter are well investigated because the search for new materials is very important for tomorrow's field of light generation for illumination. Since the pioneering work of Nakamura in 1993 [2], the blue-emitting GaN light emitting diode brought a significant revolution in lighting technology. The first commercial white-emitting LED solid-state lighting (SSL) device was developed using this blue-emitting LED in 1997 [3], combining a blue LED with the yellow yttrium aluminum garnet (YAG:Ce^{3+}) phosphor, that absorbs blue light ($\lambda \sim 460$ nm) and emits yellow light. This type of device has, however, a problem of low color reproducibility because the degradation rates of the LED and the phosphor are not isochronous, resulting in a color shift during the lifetime of the device [4,5]. Presently, the emission bands of LEDs are shifted to the near UV range, and another approach to assemble the SSL has been proposed, where a near-UV LED is combined with a mix of tri-color phosphors. The near-UV LED emits UV/violet light in the range 350–410 nm that excites the phosphors resulting in the emission of white light. Following this approach, T. Nishida et al. have assembled a SSL device using an AlGaN UV-LED as a light source (emission at 350 nm) and the three-basal color (TBC) phosphors (red Y_2O_2S:Eu; green ZnS:(Cu, Al) and blue ZnS:Ag) [6]. The color shift in these devices is reduced because the visible emission is now mainly due to the phosphors rather than from the LED, and the variations of the emission features of the TBC phosphors with temperature have similar rates.

Conventional blue and green phosphors (green ZnS:(Cu, Al) and blue ZnS:Ag) are very efficient light emitters [7,8]. However, using sulfide-base materials for this purpose has disadvantages such as chemical instability during operation, corrosion of the emitter, and sulfur related contamination [9]. To avoid these problems, these phosphors are being replaced by lanthanide-doped materials such as the green emitting phosphor $MgLaLiSi_2O_7$:Tb^{3+} and the blue emitting $BaMgAl_{10}O_{17}$:Eu^{2+} [10,11]. Red phosphors suitable for use in SSL devices are Y_2O_3:Eu^{3+}, Y_2O_2S:Eu^{3+} and YVO_4:Eu^{3+}, but since they do not have enough absorption in the near-UV region, it is necessary to use a phosphor mixture containing 80% red, 10% green and 10% blue in order to obtain good color rendering. Besides this, Y_2O_2S:Eu^{3+} phosphors are chemically unstable [12,13]. Consequently, red phosphors are, at the moment, the bottleneck for the advancement of SSL systems.

* Corresponding author at: Dpto. Química, Univ. Católica del Norte Casilla 1280/Antofagasta/Chile. Tel.: +56 55 355624; fax: +56 55 355632.
E-mail address: jllanos@ucn.cl (J. Llanos).

0925-8388/$ – see front matter © 2011 Elsevier B.V. All rights reserved.
doi:10.1016/j.jallcom.2011.01.161

In order to try to solve the aforementioned problems we have chosen rare-earth tellurates as a host lattice for new red phosphors because of their chemical and thermal stability. Ln_2TeO_6 crystallize in the orthorhombic system with space group $P2_12_12_1$, where the cations occupy two independent atomic positions and are coordinated sevenfold by oxygen in form of a square-triangle polyhedron and a capped trigonal prism, respectively. Both coordination polyhedra are characterized by the lack of inversion symmetry [14]. It is known that for Eu^{3+}cations located at a non-centrosymmetric site, the preferred transition is $^5D_0 \rightarrow {}^7F_2$ and the emission is red.

In this paper, we report the synthesis and photoluminescence spectra (emission and excitation) and the effect of the nanoparticles size on the optical properties of the new red-emitting $La_{1.90}Eu_{0.10}TeO_6$:RE $^{3+}$ (RE = Gd, Sm) and Y_2TeO_6:Eu^{3+}phosphors. All the phases were prepared by using the Pechini sol–gel process [15]. The optimizations of dopant ion concentration as well as the luminescence decay time were also investigated.

2. Experimental

2.1. Synthesis

The $La_{1.90}Eu_{0.10}TeO_6$:RE (RE = Sm^{3+}, Gd^{3+}) phosphors were prepared by the Pechini sol–gel method [15]. According to the stoichiometric formula, 4.36×10^{-3} mol of La_2O_3 (Aldrich, 99.99% pure), 2.18×10^{-4} mol of Eu_2O_3 (Aldrich, 99.99% pure) as well as Sm_2O_3 (Aldrich, 99.99% pure) or Gd_2O_3 (Aldrich, 99.99% pure) in different ratios, were dissolved in 30 ml of HNO_3 (0.5 mol dm^{-3}) under vigorous stirring. $Y_{2-x}Eu_xTeO_6$ was prepared from 4.36×10^{-3} mol of Y_2O_3 (Aldrich, 99.99% pure) and Eu_2O_3 (Aldrich, 99.99% pure) in different ratios. The pH of the solutions was adjusted between 1 and 2. When the oxides were completed dissolved, they were mixed with a water–ethanol (v/v = 1:7) solution containing citric acid (Merck, A.R) as chelating agent for the metal ions and 4.36×10^{-3} mol of H_6TeO_6 (Aldrich, 97.5–102.5% pure). In all cases, the molar ratio of telluric acid to citric acid was 1:2. Afterward, ca. 1.25 g of polyethylene glycol (PEG, M.W. = 20,000, Fluka, A.R.) was added as a cross-linking agent. Transparent sols were obtained after stirring for 2 h. The sols were dried in a 343 K water bath. When the sols were completely dry, they were annealed at 673 K in a furnace. After annealing, the resulting powders were fired to 1073 K with a heating rate of 1 K/min and kept there for two hours. Optical inspection of $La_{1.90}Eu_{0.10}TeO_6$:Sm^{3+}, $La_{1.90}Eu_{0.10}TeO_6$:Gd^{3+} and Y_2TeO_6:Eu^{3+} showed homogeneous white powders for all phases.

2.2. Characterization

To check the phase's purity, powder X-ray diffraction (PXD) patterns were collected with a Siemens D-5000 diffractometer fitted with a graphite monochromator, using Cu Kα_1 radiation, $\lambda = 0.15406$ nm. All measurements were carried out at room temperature. The surface morphology of the nanocrystalline$La_{1.90}Eu_{0.10}TeO_6$:Sm^{3+}, $La_{1.90}Eu_{0.10}TeO_6$:Gd^{3+} and Y_2TeO_6:Eu^{3+}phosphors was inspected using scanning electron microscopy (SEM, Jeol, JSM-6360 LV). FT-IR spectra were measured with a Perkin-Elmer Spectrum BX spectrophotometer with the KBr pellet technique. Raman spectra were obtained with a Witec alpha 300 microscope equipped with Confocal Raman Spectroscopy using a HeNe laser ($\lambda = 633$ nm). The accuracy of the peak position is typically 4 cm^{-1}. All measurements were carried out at room temperature. The photoluminescence (PL) spectra (emission and excitation) and fluorescence lifetime were measured using a JASCO FP-6500 spectrofluorometer. All spectra were registered at room temperature. In order to compare the photoluminescence intensity, the amount of samples was the same in all experiments.

3. Results and discussion

La_2TeO_6 and Y_2TeO_6 crystallize in the space group $P2_12_12_1$ of the orthorhombic system with four formula units in the cell of dimensions $a = 5.510(1)$ Å, $b = 9.441(2)$ Å, $c = 10.387(3)$ Å and $a = 5.2456(4)$ Å, $b = 9.0361(7)$ Å, $c = 9.9312(8)$ Å, respectively [16,17].The powder X-ray diffraction patterns of $La_{1.90}Eu_{0.10}TeO_6$ samples doped with Sm^{3+} and $Gd^{3+}$are shown in Figs. 1 and 2 respectively, and can be indexed in the orthorhombic symmetry indicating the existence of a range of solid solutions, represented by the formula $La_{1.90-x}Eu_{0.10}Sm_xTeO_6$ ($x = 0.00$, 0.02, 0.04, 0.06, 0.08, 0.10, 0.12 and 0.14) and $La_{1.90-x}Eu_{0.10}Gd_xTeO_6$ ($x = 0.00$, 0.02, 0.04 and 0.06).

On the other hand, the X-ray diffraction patterns of the samples of general formula $Y_{2-x}Eu_xTeO_6$ ($x = 0.00$, 0.02, 0.04, 0.06, 0.08, 0.10, 0.12 and 0.14) also indicate the existence of a unique range of solid solution as described above (Fig. 3). The substitution of Y^{3+} ions with Eu^{3+} ions causes an increase of the unit cell parameters in view of the fact that the ionic radii of Y^{3+} (0.96 Å) ions is slightly smaller than that of Eu^{3+} (1.01 Å) [18]. Indexing was performed using the Unit Cell software [19].

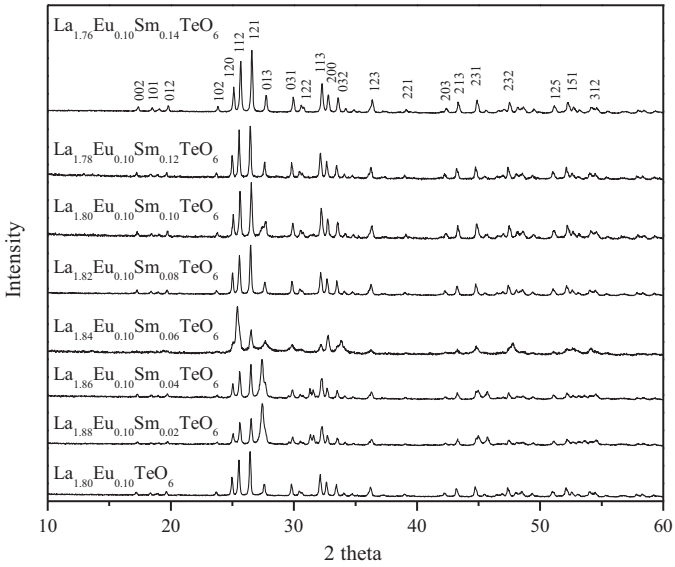

Fig. 1. XRD patterns of $La_{1.90-x}Eu_{0.10}Sm_xTeO_6$ ($x = 0$, 0.02, 0.04, 0.06, 0.08, 0.10, 0.12, 0.14).

Using the Scherrer equation it is possible to estimate the crystallite size. The Scherrer equation, $D = 0.90\lambda/\beta\cos\theta$, predicts crystallite thickness if crystals are smaller than 1000 Å. Since small angular differences in angle are associated with large spatial distances (inverse space), broadening of a diffraction peak is expected to reflect some scale feature in the crystal. In this equation D is the average grain size, λ is the wavelength of the radiation used in the diffraction experiments, θ is the diffraction angle and β is the full-width at half-maximum (FWHM) of the observed peak [20,21]. The strongest diffraction peaks (1 2 1) were used to calculate the grain sizes of the samples. ($D_{Y_{1.86}Eu_{0.14}TeO_6} = 52$ nm, $D_{La_{1.88}Eu_{0.10}Sm_{0.02}TeO_6} = 43$ nm, $D_{La_{1.88}Eu_{0.10}Gd_{0.020}TeO_6} = 62$ nm).

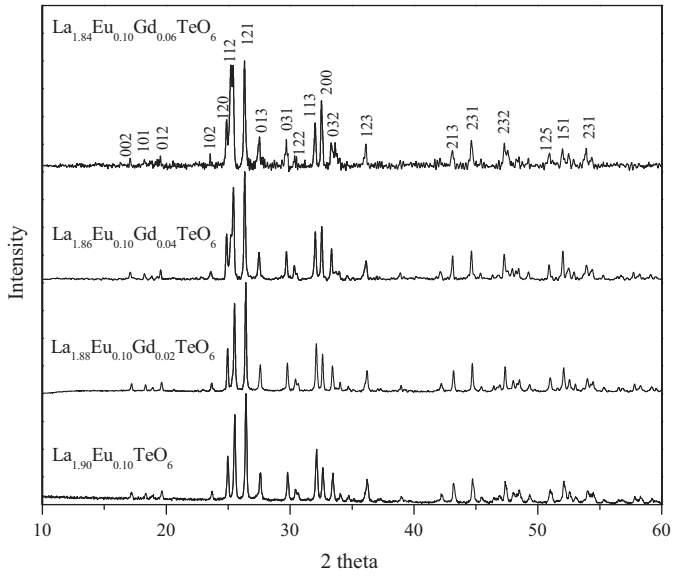

Fig. 2. XRD patterns of $La_{1.90-x}Eu_{0.10}Gd_xTeO_6$ ($x = 0.02$, 0.04 and 0.06).

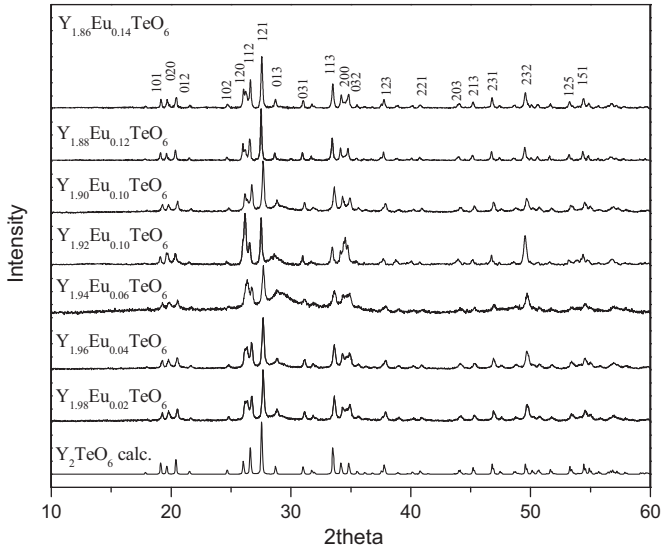

Fig. 3. XRD patterns of $Y_{2-x}Eu_xTeO_6$ ($x = 0.02$, 0.04, 0.06 and 0.10).

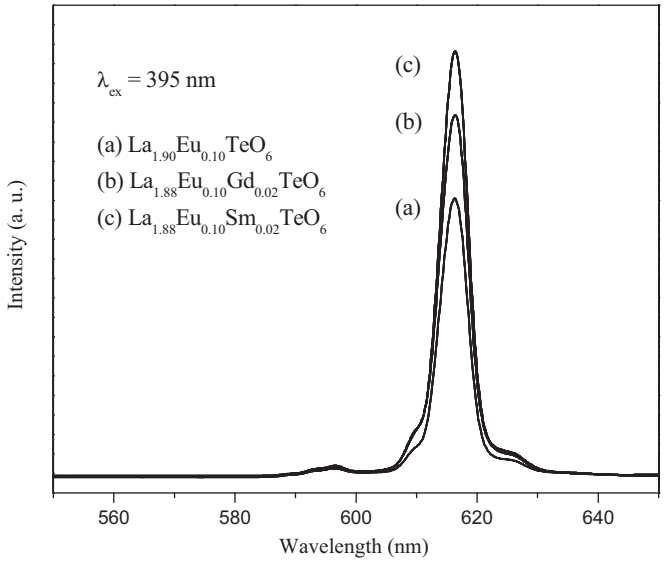

Fig. 5. Emission spectra of 1 mol% Gd^{3+} or Sm^{3+} doped $La_{1.90}Eu_{0.10}TeO_6$. ($\lambda_{ex} = 395$ nm) ((a) $La_{1.90}Eu_{0.10}TeO_6$; (b) $La_{1.88}Eu_{0.10}Gd_{0.02}TeO_6$; (c) $La_{1.88}Eu_{0.10}Sm_{0.02}TeO_6$).

The morphology of the crystallites was inspected using scanning electron microscopy (SEM). These studies reveal that the samples show a strong tendency to form agglomerates, as shown in Fig. 4.

3.1. Photoluminescence spectra of $La_{1.90}Eu_{0.10}TeO_6$ samples doped with Gd^{3+}/Sm^{3+}

The photoluminescence spectra of $La_{1.90-x}Eu_{0.10}Gd_xTeO_6$ ($x = 0.00$, 0.02, 0.04, 0.06) and $La_{1.90-x}Eu_{0.10}Sm_xTeO_6$ ($x = 0.02$, 0.04, 0.06, 0.08, 0.10, 0.12 and 0.14) show a strong $^5D_0 \rightarrow {}^7F_2$ emission line on excitation at 395 nm. In order to improve the emission efficiency of $La_{1.90}Eu_{0.10}TeO_6$ we have replaced some of the Eu^{3+} ions by Gd^{3+} or Sm^{3+}cations. From comparison of the emission intensity of the samples with different concentration of Gd^{3+} or Sm^{3+} doped concentration, the luminescence reaches the maximum intensity with the following compositions $La_{1.88}Eu_{0.10}Gd_{0.02}TeO_6$ and $La_{1.88}Eu_{0.10}Sm_{0.02}TeO_6$. It is observed that the quenching concentration is lower in the nanocrystalline samples than in the bulk ones [22]. The emission spectra for the optimized phosphors are shown in Fig. 5. The excitation spectra for monitoring the $^5D_0 \rightarrow {}^7F_2$ emission of Eu^{3+} show an absorption in the short-wavelength region (250–270 nm) plus the sharp bands centered at 395.6 nm, 466 nm, and 534.6 nm. These sharp excitation peaks are assigned to the typical $4f^n \rightarrow 4f^n$ transitions of Eu^{3+}. According to previous works, the excitation around 395 nm corresponds to $^7F_0 \rightarrow {}^5L_6$ transition, the excitation at 466 nm corresponds to $^7F_0 \rightarrow {}^5D_2$ transition and finally the excitation around 534 nm corresponds to $^7F_0 \rightarrow {}^5D_1$ transition [23]. The excitation spectrum of the sample containing Sm^{3+} shows also a sharp $^6H_{5/2} \rightarrow {}^4K_{11/2}$ line at 406 nm [24] (see Fig. 6).

The luminescence intensities of $^5D_0 \rightarrow {}^7F_2$ emission line (618 nm) on excitation at 395 nm are found to be highly dependent of the co-dopant concentration. The emission intensity reaches the peak maximum at a co-dopant concentration (Gd^{3+} or Sm^{3+}) of 1 mol% (Fig. 7). The decay curves of the $^5D_0$ luminescence in the $La_{1.88}Eu_{0.10}Gd_{0.02}TeO_6$ and $La_{1.88}Eu_{0.10}Sm_{0.02}TeO_6$ nanocrystals are shown in the respective inset. These curves are well fitted to a mono-exponential function and can be represented by $I = I_0 \exp(t/\tau)$, where I and I_0 are the luminescence intensities at time t and 0 and τ represents the radiative decay time [25]. The results show that the decay mechanism of the $^5D_0 \rightarrow {}^7F_2$ transition is due only to the Eu^{3+} ions in the structure, which are homogeneously distributed inside the host lattice without surface defects. When we compared the optical properties of the nanocrystalline phosphors

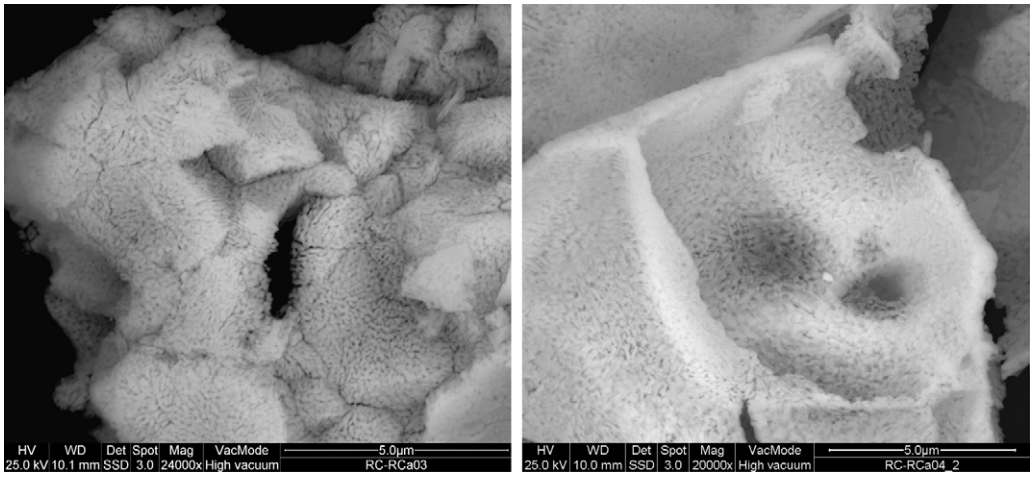

Fig. 4. SEM micrography of $La_{1.88}Eu_{0.10}Sm_{0.02}TeO_6$ prepared by Pechini sol–gel method.

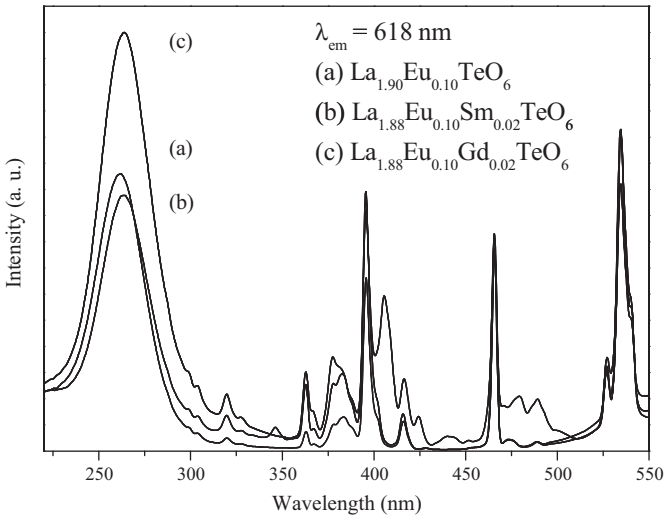

Fig. 6. Excitation spectra of 1 mol% Gd^{3+} or Sm^{3+} doped $La_{1.90}Eu_{0.10}TeO_6$. (λ_{em} = 618 nm). ((a) $La_{1.90}Eu_{0.10}TeO_6$; (b) $La_{1.88}Eu_{0.10}Sm_{0.02}TeO_6$; (c) $La_{1.88}Eu_{0.10}Gd_{0.02}TeO_6$).

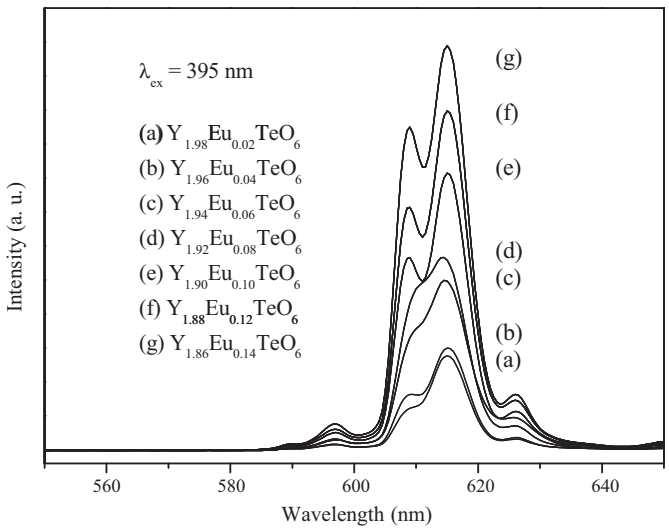

Fig. 8. Emission spectra of $Y_{2-x}Eu_xTeO_6$ (x = 0.02, 0.04, 0.06, 0.08, 0.10, 0.12, and 0.14) prepared by Pechini sol–gel method (λ_{ex} = 395 nm).

prepared by the Pechini process with respect to the phosphors prepared by conventional solid state methods we found that the nanocrystalline phosphors show a better colorimetric resolution, with the FWHM of the emission spectra narrower than in the bulk samples [26].

3.2. *Photoluminescence and Raman spectra of Y_2TeO_6 samples doped with Eu^{3+}*

The emission spectra of Eu^{3+}-doped phosphors $Y_{2-x}Eu_xTeO_6$ upon excitation with light of 395 nm are shown in Fig. 8. The spectra are comparable to that of Eu^{3+} in $La_{1.88}Eu_{0.10}Gd_{0.02}TeO_6$and $La_{1.88}Eu_{0.10}Sm_{0.02}TeO_6$, except that the emission can be divided into two bands, with the magnitude of the splitting depending on the concentration of Eu^{3+}.

The luminescence intensities of the $^5D_0 \rightarrow {}^7F_2$ emission line (618 nm) on excitation at 395 nm are found to be not dependent on the dopant concentration. The emission intensity reaches the peak maximum when the Eu^{3+}concentration is 7 mol%.

The concentration dependence of the Eu^{3+} emission intensities is illustrated in Fig. 9. The phenomenon of concentration quenching is not observed in these phosphors, since the energy transfer between the luminescent centers is not efficient enough. The lifetime of the Eu^{3+} emission increases slightly with a low Eu^{3+} concentration, but a significant decrease of the decay time is observed at high concentrations of the activator cation.

In order to investigate if the doping of Eu^{3+} ions alters the host structure, we performed the FT-IR and Raman spectra of Y_2TeO_6 and $Y_{1.86}Eu_{0.14}TeO_6$ (Fig. 10). The Raman and IR spectra supported the existence of $TeO_6{}^{6-}$ groups in the structure [26]. In the crystal structure of Y_2TeO_6, the Te^{6+} ions occupy the 4(a) positions with site symmetry $C_1$with six oxygen atoms in a shape of a distorted octahedron surrounding the Te^{6+}cations [17]. As a consequence of the lack of symmetry all vibrational modes may be found in the Raman, as well as in the IR spectra [27]. The peak positions are listed in Table 1. The assignments of the vibrational absorptions were made starting from the results of Siebert for the $TeO_6{}^{6-}$ anion in $PbMnTeO_6$ [28]. The results show that υ_1 of $Y_{1.84}$ $Eu_{0.16}TeO_6$ (749 cm^{-1}) is larger than that of Y_2TeO_6 (744 cm^{-1}). The differenti-

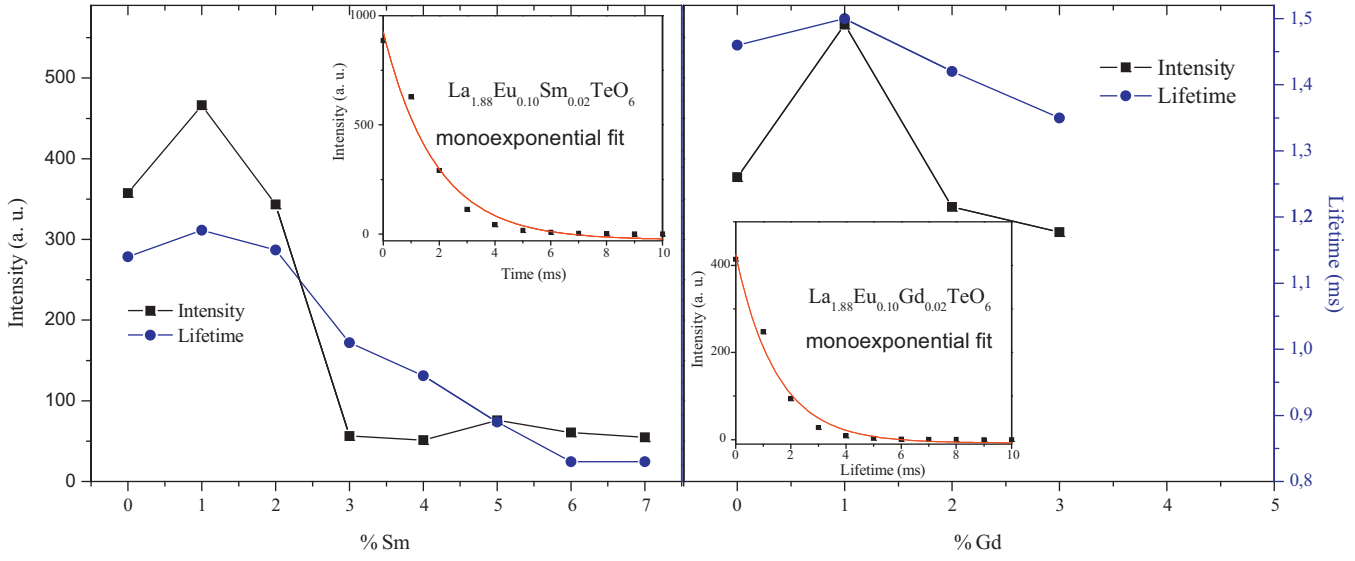

Fig. 7. The dependence of Sm^{3+} (left) or Gd^{3+} (right) emission intensity (λ_{em} = 618 nm) on the concentration of Sm^{3+} or Gd^{3+} in $La_{1.90}Eu_{0.10}TeO_6$. Decay curves of the $^5D_0$ luminescence of the Eu^{3+}in the respective phosphors (inset).

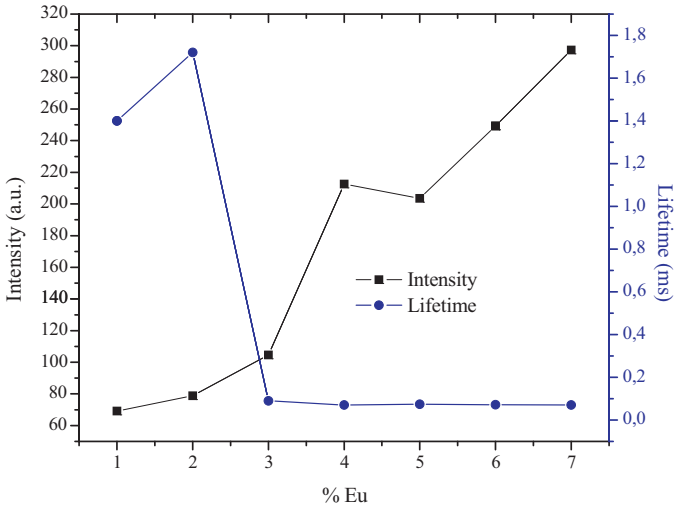

Fig. 9. The emission intensity and decay time of Eu^{3+} as a function of doping concentration under an excitation of 395 nm. The signals were detected at 618 nm.

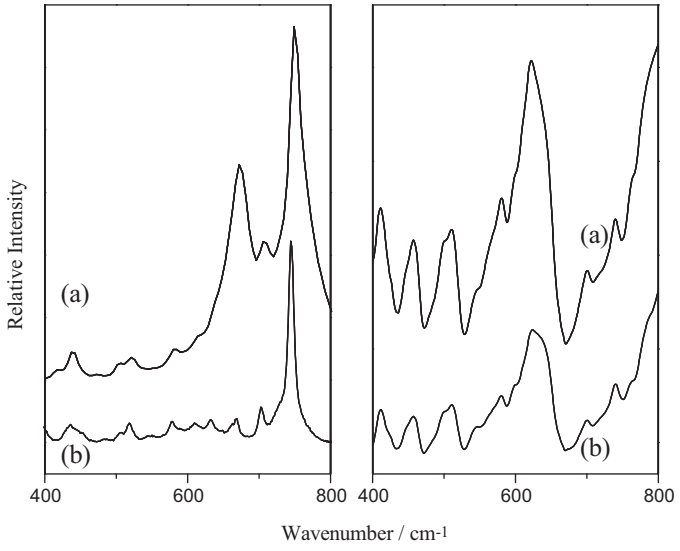

Fig. 10. Raman (left) and FT-IR (right) spectra of (a) $Y_{1.86}Eu_{0.14}TeO_6$ and (b) Y_2TeO_6.

Table 1
Assignment of the IR and Raman spectra of Y_2TeO_6 and $Y_{1.86}Eu_{0.14}TeO_6$ (bands in cm^{-1}).

Vibration	Y_2TeO_6		$Y_{1.86}Eu_{0.14}TeO_6$	
	IR	Raman	IR	Raman
ν_1	754 w	744 vs	759 w	749 vs
ν_2	667 vs	669 w	671 vs	672 w
ν_3	732 m	702 m	740 m	703 m
ν_4	590 w, 606 w	579 w, 610 w	594 w, 609 w	580 w, 613 w
ν_5	490 m, 506 w	505 w, 518 w	498 m, 511 w	506 w, 521 w

ation could be related with the difference of the ionic radii between Eu^{3+} and Y^{3+}. The Raman and IR spectra confirm the existence of a unique range of solid solution (vide supra).

4. Conclusions

Nanocrystalline $La_{1.90}Eu_{0.10}TeO_6$:RE $^{3+}$ (RE = Gd, Sm) and Y_2TeO_6:Eu^{3+}phosphors were successfully prepared by the Pechini sol–gel process using as starting products the lanthanide sesquioxides and telluric acid. XRD results indicate the existence of a range of solid solutions for all phases. Its photoluminescence spectra were measured at room temperature. Co-doping of Gd^{3+} or Sm^{3+} in $La_{1.90}Eu_{0.10}TeO_6$ enhances the red emission at 618 nm when the concentration of Gd^{3+} or Sm^{3+}reaches the 1 mol% limit. The maximum value is observed for the Gd^{3+}-containing phosphor.

On the other hand, the photoluminescence behavior presents similar features, indicating that the RE^{3+} ions are found in the same symmetry site (C_1) in all phases, which is corroborated in the case of $Y_{2-x}Eu_xTeO_6$ by IR and Raman spectra.

Finally, the study reveals that the optimized phosphors could be used as red components for white lighting devices excited in the near UV region using the InGaN–LED as exciting source.

Acknowledgment

This work was supported by FONDECYT-CHILE (grant 1090327).

References

[1] T. Jüstel, H. Nikols, C. Ronda, Angew. Chem. Int. Ed. 37 (1998) 3084.
[2] S. Nakamura, M. Senoh, T. Mukai, Appl. Phys. Lett. 62 (1993) 2390.
[3] S. Nakamura, G. Fasol, The Blue Laser Diode, Springer, Berlin, 1997.
[4] C.F. Guo, Y. Xu, F. Lv, X. Ding, J. Alloys Compd. 497 (2010) L21.
[5] L. Zhou, J. Wei, J. Wu, F. Gong, L. Yi, J. Huang, J. Alloys Compd. 476 (2009) 390.
[6] T. Nishida, T. Ban, N. Kobayashi, Appl. Phys. Lett. 82 (2003) 3817.
[7] M. Ollinger, V. Cracium, K. Singh, Appl. Phys. Lett. 80 (2002) 1927.
[8] S.H. Sohn, Y. Hamakawa, Appl. Phys. Lett. 62 (1993) 2242.
[9] L. Zhou, J. Huang, F. Gong, Y. Lan, Z. Tong, J. Sun, J. Alloys Compd. 495 (2010) 268.
[10] G. Seeta Rama Raju, S. Buddhudu, Mater. Lett. 62 (2008) 1259.
[11] B.M.J. Smets, J.G. Verlijsdonk, Mater. Res. Bull. 21 (1986) 1305.
[12] S. Neeraj, N. Kijima, A.K. Cheetham, Solid State Commun. 131 (2004) 65.
[13] X.-x. Wang, J. Wang, J.-x. Shi, Q. Su, M.-I. Gong, Mater. Res. Bull. 42 (2007) 1669.
[14] M. Trömel, F.W. Hützler, H.G. Burckhardt, C. Platte, E. Münch, Z. Anorg, Allg. Chem. 551 (1987) 95.
[15] M.P. Pechini, U.S. Patent 3,330,697 (1967).
[16] S.F. Meier, T. Schleid, J. Solid State Chem. 171 (2003) 408.
[17] P. Höss, T. Schleid, Acta Crystallogr. E-Struct. Rep. (2007) 63–65, i133.
[18] R.D. Shannon, Acta Cryst. A32 (1976) 751.
[19] T.J.B. Holland, S.A.T. Redfern, Miner. Mag. 61 (1977) 65.
[20] A.L. Patterson, Phys. Rev. 56 (1939) 978.
[21] Y.W. Wang, Y. Yang, S. Jin, S.J. Tian, G.B. Li, J.T. Jia, C.S. Liao, C.H. Yan, Chem. Mater. 13 (2001) 372.
[22] R. Castillo, J. Llanos, J. Lumin. 128 (2009) 465.
[23] C.A. Kodaira, H.F. Brito, O.L. Malta, O.A. Serra, J. Lumin. 101 (2003) 11.
[24] C.A. Kodaira, R. Stefani, A.S. Maia, M.C.F.C. Felinto, H.F. Brito, J. Lumin. 127 (2007) 616.
[25] D.R. Vij, Luminescence of Solids, Plenum Press, New York, 1998.
[26] R. Castillo, J. Llanos, J. Lumin. 129 (2009) 465.
[27] J. Llanos, R. Castillo, D. Barrionuevo, D. Espinoza, S. Conejeros, J. Alloys Compd. 485 (2009) 565.
[28] H. Siebert, Z. Anorg. Allg. Chem. 301 (1959) 161.